



GEORG-AUGUST-UNIVERSITÄT  
GÖTTINGEN



Georg-August-University  
of Goettingen

## Tracking Performance Analysis for the ZEUS-Detector

DESY Summerstudent Programme 2008  
Supervisor: Achim Geiser

by  
Katharina Fiekas  
Hannoversche Str.134  
37077 Göttingen  
September 15, 2008

### **Abstract**

The following report belongs to my work at DESY as a summerstudent, where I do some analysis on the tracking before the starting of the grand reprocessing.



# Contents

<b>1</b>	<b>Introduction</b>	<b>1</b>
<b>2</b>	<b>The HERA ring</b>	<b>2</b>
2.1	The ZEUS detector . . . . .	4
<b>3</b>	<b>Event reconstruction and selection</b>	<b>6</b>
3.1	Tracking and Vertex finding . . . . .	6
3.2	Particle Selection . . . . .	6
3.2.1	Invariant mass . . . . .	7
<b>4</b>	<b>Datasets</b>	<b>8</b>
<b>5</b>	<b>Tracking studies on <math>J/\Psi</math></b>	<b>9</b>
5.1	$J/\Psi$ . . . . .	9
5.2	The Cuts . . . . .	10
5.3	Invariant mass spectrum for the two muons . . . . .	12
5.3.1	Resolution studies for the different datasets . . . . .	13
5.4	Detector resolution . . . . .	14
5.5	Searches for $Z^0$ -candidates . . . . .	15
5.5.1	$Z^0$ . . . . .	15
5.5.2	Invariant mass spectrum for the two muons . . . . .	16
<b>6</b>	<b>Tracking studies on <math>D^*</math></b>	<b>21</b>
6.1	$D^*$ . . . . .	21
6.2	The Cuts . . . . .	22
6.3	$\Delta M$ spectrum . . . . .	23
6.3.1	Resolution studies for the different datasets . . . . .	24
<b>7</b>	<b>Conclusion</b>	<b>26</b>
<b>8</b>	<b>Acknowledgements</b>	<b>27</b>
	<b>Bibliography</b>	<b>28</b>
	<b>List of Figures</b>	<b>28</b>
	<b>List of Tables</b>	<b>29</b>
<b>A</b>	<b>Measurement results</b>	<b>31</b>



# 1 Introduction

In HERA Physics one wants to measure for example the proton structure or the heavy quark production and many other things. Many of these measurements need a measurement of particle momenta, so one needs a good tracking performance.

For studies of the tracking, a good way is to look at  $J/\Psi$  or  $D^*$  candidates. There is no possibility that the tracking has an efficiency of 100%, because there is background and some of these processes look like right events.

The following analysis was done for the different time periods of data taking, because there will be a grand reprocessing, which is not yet ready.

## 2 The HERA ring

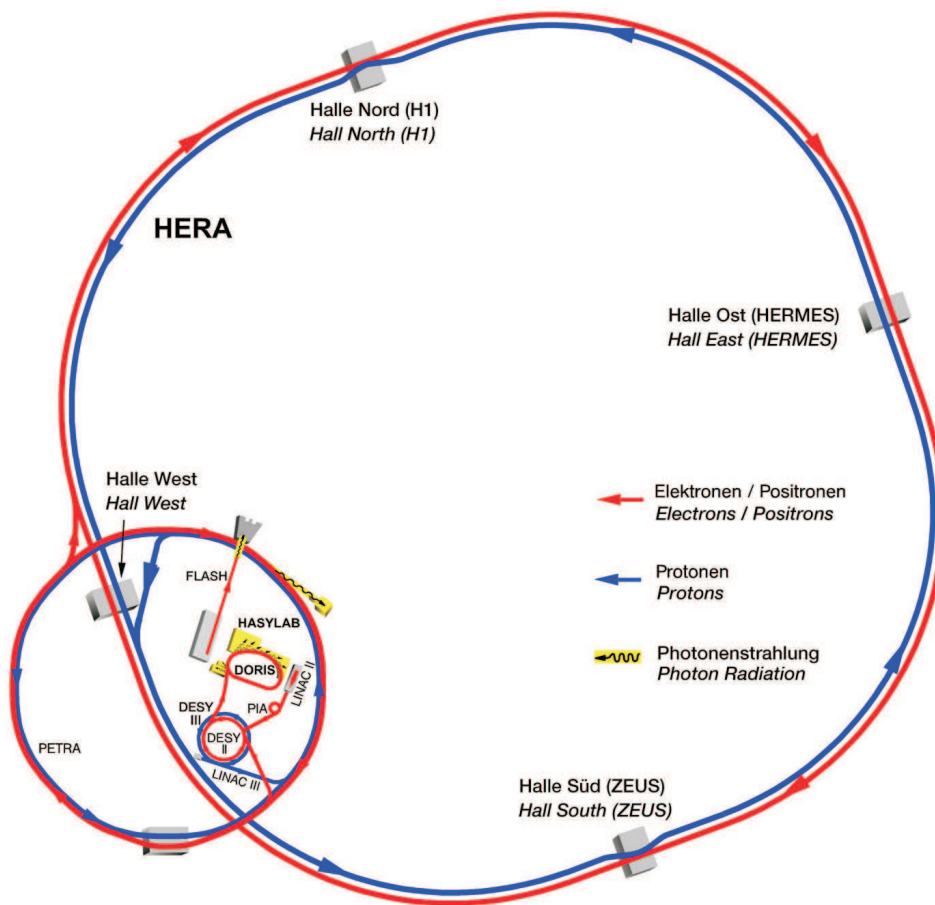


Figure 2.1: The HERA-Ring [1]

The HERA accelerator is a  $e^\pm p$  collider, where the electrons or positrons have an energy of 27.5 GeV and the protons have an energy of 920 GeV since 1998. Therefore the center of mass energy is 318 GeV. Fig.2.1 shows the HERA ring with its pre-accelerators and its 4 experiments(ZEUS, H1, HERMES and HERA-B)

In the collisions the interactions took place over the exchange of a gauge boson, between the electron or positron with one parton of the proton. The gauge boson can be a photon as well as a  $W^{+/-}$  or a  $Z^0$  boson.

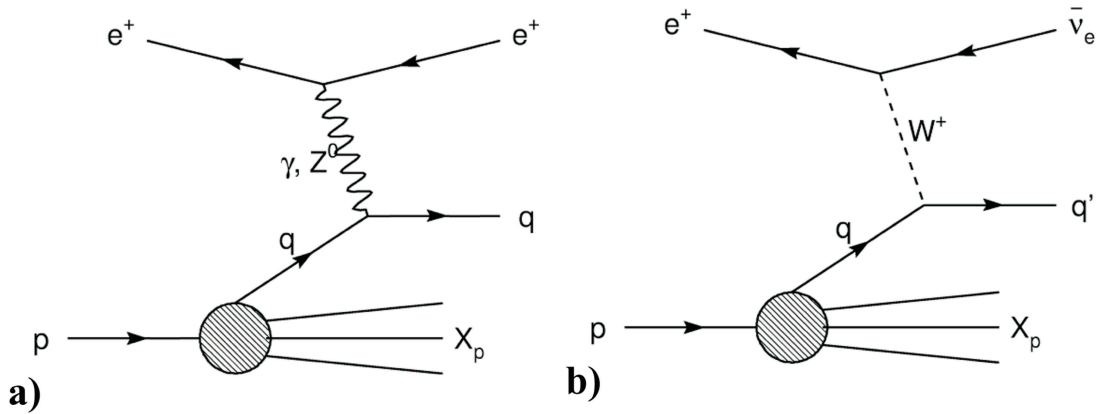


Figure 2.2: Feynman graphs of the  $e^\pm p$  scattering at the HERA a) neutral current b) charged current [5]

Depending on the virtuality  $Q^2$  of the gauge boson, which is given by the momentum of the incoming electron or positron ( $e$ ) and the momentum of the outgoing electron or positron for the neutral current or the neutrino for the charge current ( $e'$ )

$$Q^2 = -q^2 = (e - e')^2,$$

there is a difference between two processes:

- $Q^2 \approx 0 \text{ GeV}^2$ : photoproduction: the exchange boson is nearly real
- $Q^2 \geq 1 \text{ GeV}^2$ : deep inelastic scattering (DIS)

## 2.1 The ZEUS detector

The ZEUS [7] detector is the biggest experiment at the HERA ring with a dimension of  $12\text{ m} \times 10\text{ m} \times 19\text{ m}$ . It is a multipurpose detector and because of the kinematic situation of the HERA collider it had a small asymmetry (fig.2.3).

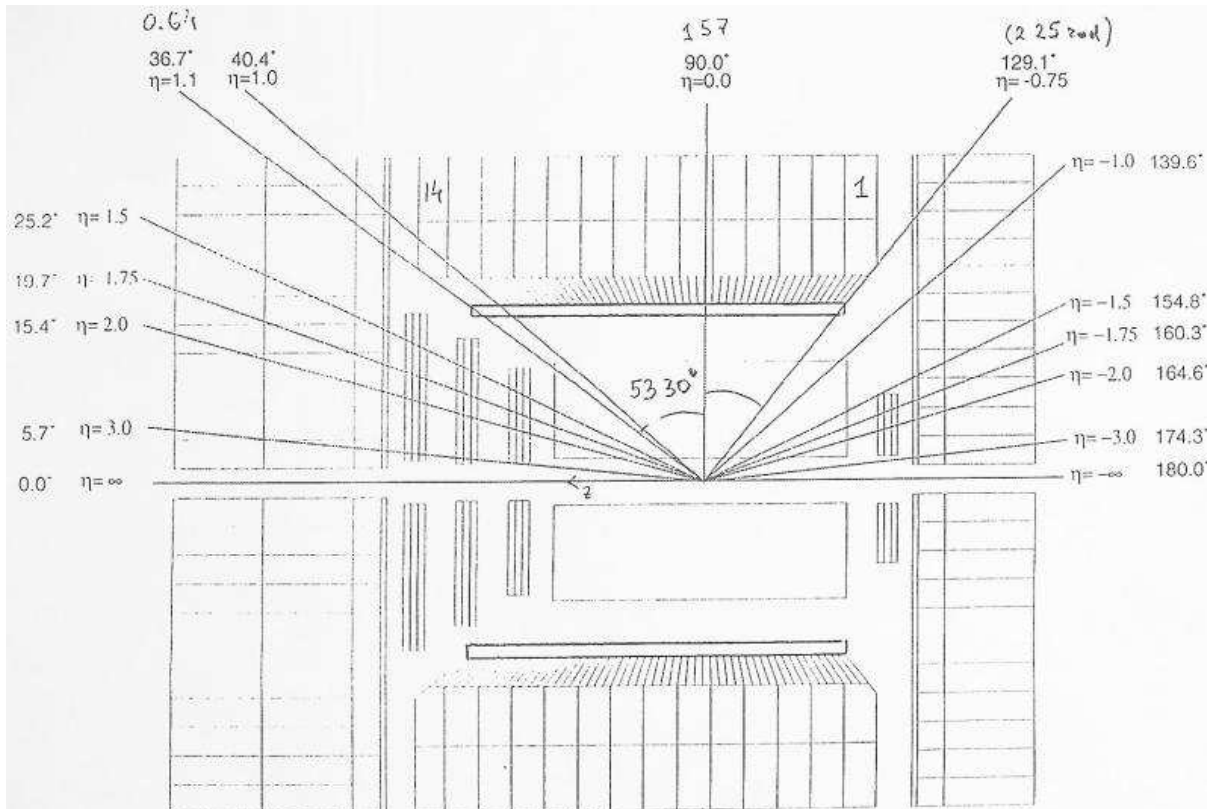


Figure 2.3: The  $\eta$  range of the ZEUS detector [2]

The main components of the ZEUS detector (fig.2.4 and fig.2.5) were the uranium scintillator calorimeter (CAL) in the heart of the detector, which enclosed the tracking chambers and was covered by a thin superconducting solenoid, the backing calorimeter (BAC) and the muon chambers (MUON).

The tracking chambers measured the tracks of the charged particles and included the vertex detector (MVD, formally VXD), the central drift chamber (CTD), the forward (FTD) and backward (RTD) drift chambers and in the forward direction a transition radiation detector (TRD), which were replaced in 2001 by the Straw tube tracker (STT).

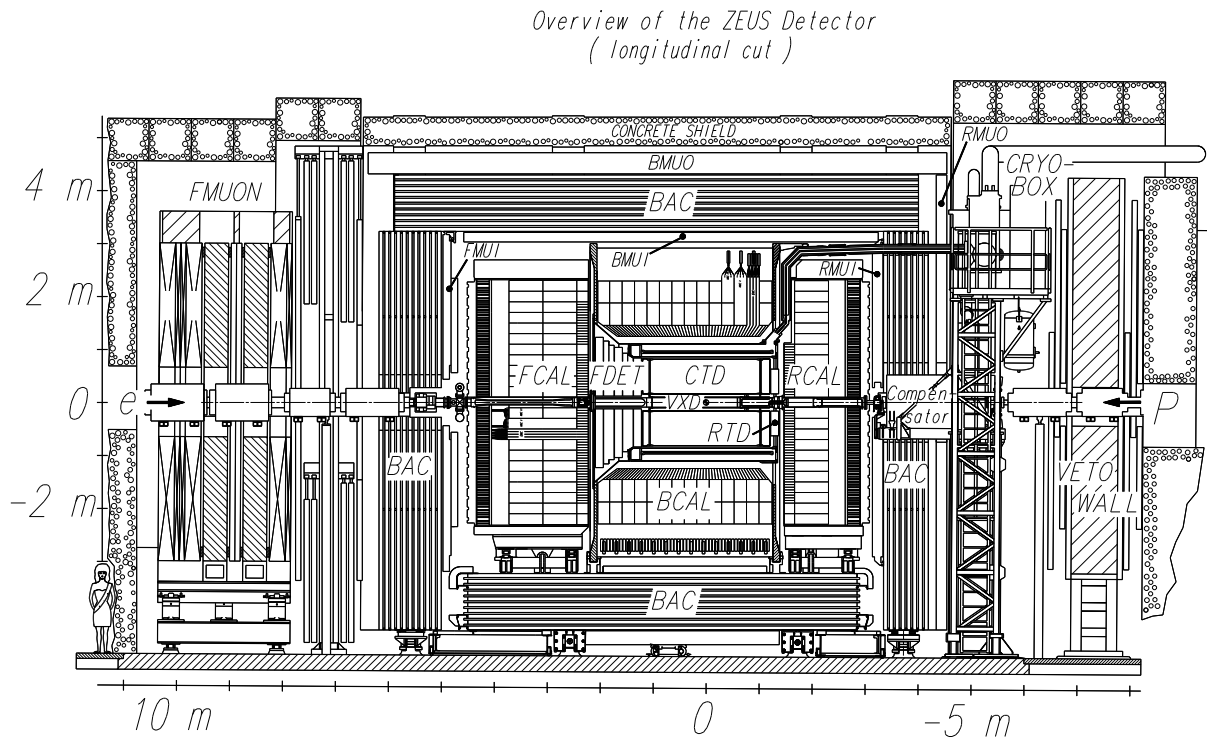


Figure 2.4: Longitudinal cut through the ZEUS detector[3]

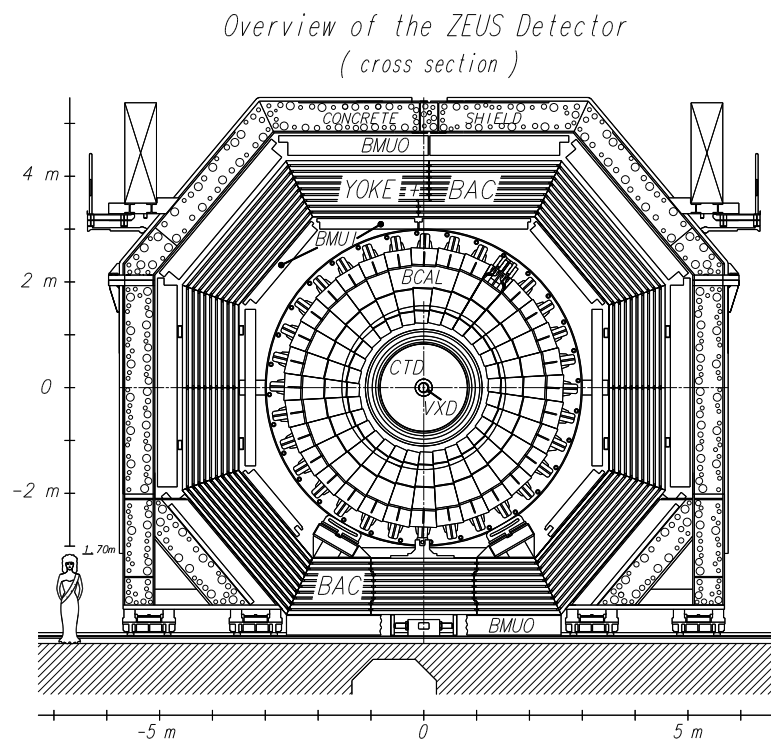


Figure 2.5: Lateral cut through the ZEUS detector[3]

# 3 Event reconstruction and selection

In this chapter the different methods of tracking and reconstructing particles are shown.

## 3.1 Tracking and Vertex finding <sup>1</sup>

As per discription in chapter 2.1, the tracking system in ZEUS consisted of the Central (CTD), the Forward (FTD), the Rear Tracking Detector (RTD), the Micro-Vertex Detector (MVD) and the Straw Tube Tracker (STT) since 2001.

First of all for the track reconstruction, there were a reconstruction of the coordinates and after that a track findig, which is called Pattern Recognition and is combining information from the MVD and CTD. In this Analysis there is a look at two different tracking modes, the regular tracking (REG) and the ZTT tracking.

- REG: Tracking mode uses the Micro Vertex Detector and the Central Tracking Detector and for the reconstruction of the tracks VCTRAK. In this case the hits were grouped into candidates for the track reconstruction and the track were fitted by connecting the hits beginning at the outer superlayer to the inner superlayer with a simple helix fit.
- ZTT: Tracking mode uses also the Micro Vertex Detector and the Central Tracking Detector but uses Kalman filtering (KFFIT) for fitting tracks. The Kalman Filter is a recursive dynamic algorithm that estimates the states for a time discrete linear system and minimize the average error.

The track fitting with the Kalman Filter evaluates each hit separatly compared to the regular tracking, where all hits are fitted at the same time.

After fitting the tracks, the verticies were identified and fitted. From that point it is possible to start with higher level analysis.

## 3.2 Particle Selection

There are many ways to reconstruct particles. Which one has to be chosen depends on the properties of the particle, for example its decays. Good ways for particle selections are to look at their energy loss because of ionisation or to calculate the invariant mass of their decay particles. Here the reconstruction is only done by the calculation of the invariant mass.

---

<sup>1</sup>used literature [10], [6], [8] and [11]

### 3.2.1 Invariant mass

The invariant mass describes the energy and the mass of a system of particles. In the laboratory system the invariant mass can be calculated from the total energy of the system.

$$m^2 = E^2 - ||p||^2$$

## 4 Datasets

For the studies in this note four datasets (03/04, 05, 06, 06/07) were used, which have got different properties.

- (03/04): The dataset 03/04 comes from collisions between positrons and protons. For the following analysis the 1<sup>st</sup> reprocessing of the data of this time period with REG was used.
- (05): The dataset 05 comes from collisions between electrons and protons and for analysis also the 1<sup>st</sup> reprocessing of the data with REG or ZTT and no STT was used. The regular tracking were used for the GMUON block and the ZTT tracking for the Dstar block of the common ntuples.
- (06): The dataset 06 comes also from collisions with electrons, but in this case for the analysis the pre-reprocessing data with REG was used.
- (06/07): The dataset 06/07 were the last data which were taken by the ZEUS detector and comes from collisions between positrons and protons. Here only a partial dataset of the data which were taken in 07 was used. They were reprocessed with the latest alignment with ZTT and rfit to test it before the grand reprocessing.

The datasets from 03/04 and 06e only includes events with muon candidates, which came from the so-called GMUON ntuples. In contrast the dataset from 05 and 06/07p includes all events, which came from the so-called common ntuples.

With the grand reprocessing there will be a unification of the datasets.

# 5 Tracking studies on $J/\Psi$

## 5.1 $J/\Psi$

The Feynman graph for  $J/\Psi$  production and its decay is shown in fig.5.1.

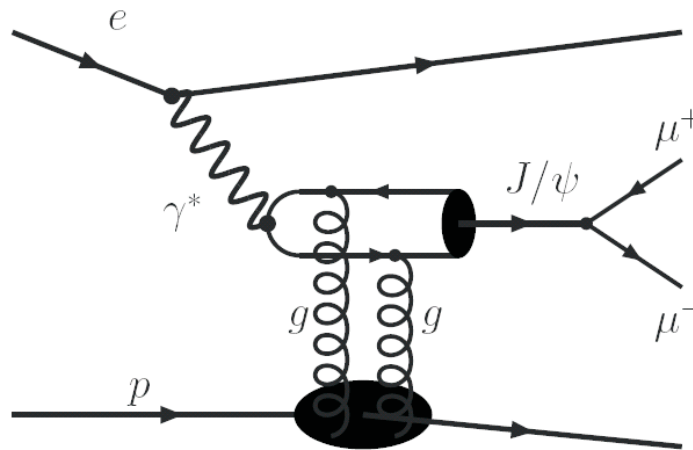


Figure 5.1:  $J/\Psi$  production and decay [13]

The branching ratios of the  $J/\Psi$  are

- $J/\Psi \rightarrow \text{hadrons}:(87.7 \pm 0.5)\%$
- $J/\Psi \rightarrow e^+e^-:(5.94 \pm 0.06)\%$
- $J/\Psi \rightarrow \mu^+\mu^-:(5.93 \pm 0.06)\%$

So the best way to reconstruct the  $J/\Psi$  Peak is to calculate the invariant mass of two unlike-signed electrons or two unlike-signed muons. In this study only events with Muon candidates were used. In fig.5.2 the invariant mass is shown for the data of 2005.

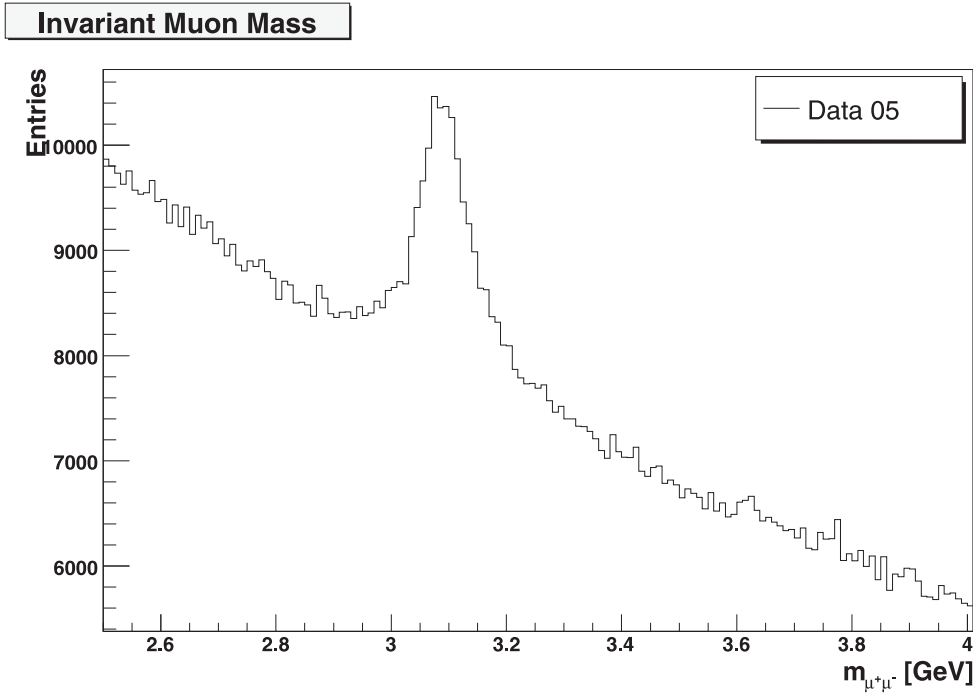


Figure 5.2: Dimuon spectrum for the dataset of 05

The initial ratio between the signal and the background is very bad, so it has to be improved by some cuts.

## 5.2 The Cuts

For the  $J/\Psi$  selection only the "best"<sup>1</sup> muon pair in each event was used. This was done by a loop over all muon combinations and there by looking for the muon pair with the highest muon quality in sum.

In the best possibility there are only two tracks, which come from the vertex and belong to two muons, but in most cases there are more than two tracks. Therefore there were more cuts down on the muon quality (Muqual) depending on the number of tracks (Ntrk):

- $N_{trk} \leq 3$ : no cuts
- $3 < N_{trk} \leq 10$ :  $Muqual \geq 2$ ,  $Sum \geq 6$
- $N_{trk} > 10$ :  $Muqual \geq 4$ ,  $Sum \geq 8$

The muon quality is an estimator of the expected signal to background ratio.

Because the reconstruction is done by requiring two muons, there is a big background which comes from cosmic muons. The property of a cosmic muon is that it goes straight through the detector, and in most cases doesn't cross the interaction point. In fig.5.3 is an example of a cosmic muon shown in the event display.

<sup>1</sup>"best" at this point means the muons with highest qualities

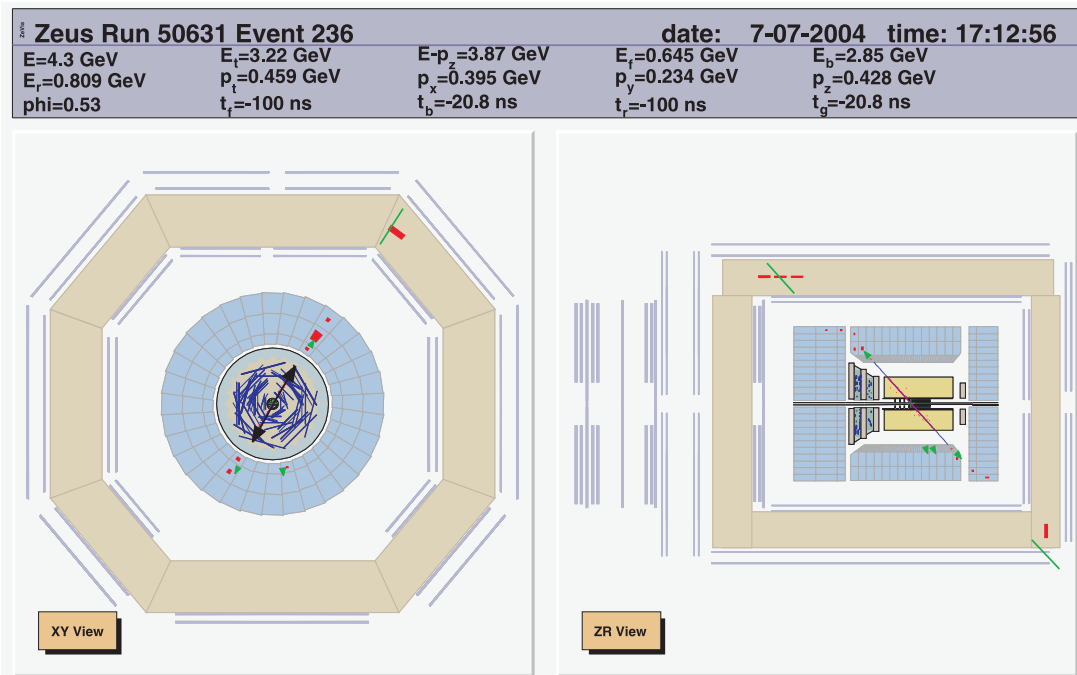


Figure 5.3: Cosmic muon event

To differentiate between muons which come from the interaction and cosmic muons one can look at the time when the muons were detected in the muon chambers. Here muons were produced in pairs, if the muons came from the interaction point they would be detected at nearly the same time in the muon chambers. For a cosmic muon there is a signal first in the upper part of the detector and later a signal in the lower part. So there are some anti-cosmic cuts

- $|\text{global time}| \leq 7 \text{ ns}$
- $\text{updown}^2 > -10 \text{ ns}$
- angle cut<sup>3</sup>

Furthermore, the vertex ought to be next to the center of the detector, so there are also some vertex cuts

- presence of a vertex
- $|\text{vertex}_z| < 50 \text{ cm}$
- $|\text{vertex}_x^2 + \text{vertex}_y^2| < 25 \text{ cm}^2$

<sup>2</sup>time difference between the muon which was detected in the upper part of the detector and the muon which was detected in the lower part of the detector

<sup>3</sup>only muons which didn't go straight through the detector

If there are more than 5 muon candidates or no energy deposition in the hadron calorimeter the tracks have to belong to the vertex. To reduce the background furthermore there were also a cut on the asymmetry of the transverse momentum of both muons ( $pt_{\text{asym}} < 0.3$ ), a cut on the consistency of the momentums of both muons in z-direction ( $\sum_{i=1}^2 p_{iz}$ ) and a cut against the noise in forward direction.

The remaining background is irreducible and comes mostly from the Bethe-Heitler-Process (fig.5.4).

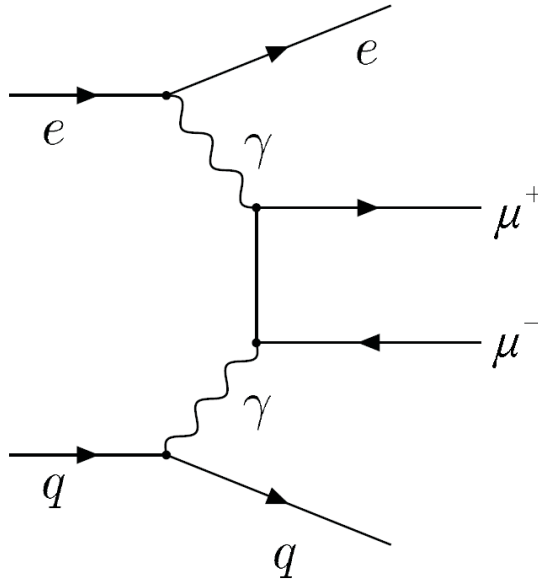


Figure 5.4: The Bethe-Heitler-Process [9]

### 5.3 Invariant mass spectrum for the two muons

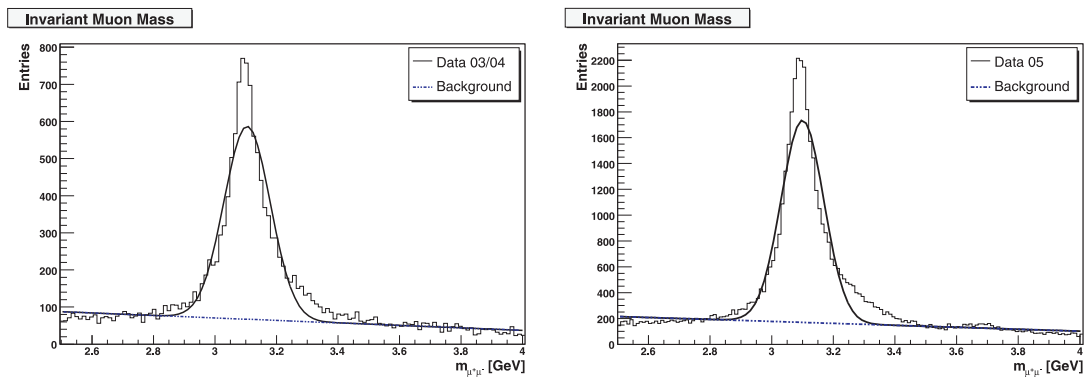


Figure 5.5: Dimuon spectrum for the dataset of a) 03/04 and b) 05

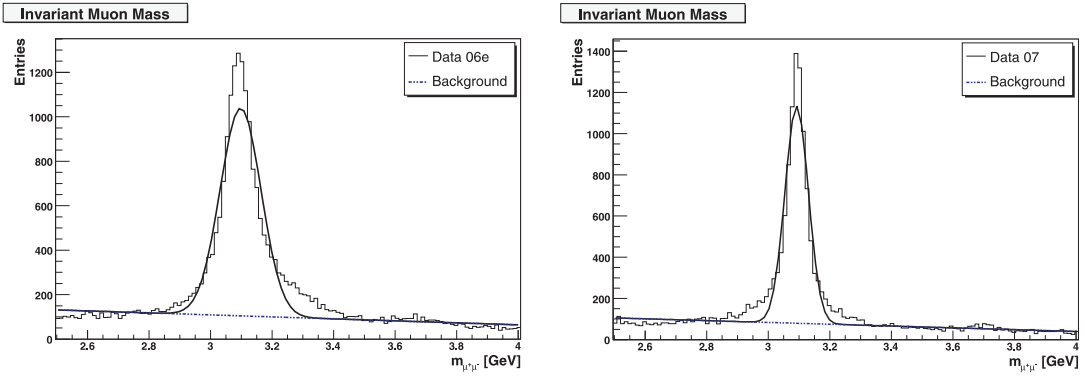


Figure 5.6: Dimuon spectrum for the dataset of a) 06e and b) 07p

In fig.5.5 to fig.5.6 the histograms for the different datasets are shown. The fits with the following function

$$f(x) = \frac{A}{\sqrt{2\pi}\sigma} e^{-\frac{1}{2}\cdot\left(\frac{x-\mu}{\sigma}\right)^2} + mx + b, \quad (5.1)$$

which are shown in this plots were done for a small range, so the background could be assumed as linear. It therefore consists of a Gaussian distribution combined with a linear distribution.

Additionally there was produced a list for each dataset which includes the run number and the event number for the entries of the histograms to simplify the following studies with this datasets.

### 5.3.1 Resolution studies for the different datasets

dataset	$\sigma$ [MeV]	$\mu$ [GeV]	$A$ [GeV]	$m$ [1/GeV]	$b$
03/04	$75 \pm 2$	$3.105 \pm 0.002$	$98 \pm 2$	$-33 \pm 2$	$171 \pm 6$
05	$69 \pm 1$	$3.100 \pm 0.001$	$272 \pm 2$	$-76 \pm 3$	$405 \pm 8$
06e	$67 \pm 1$	$3.098 \pm 0.001$	$156 \pm 2$	$-45 \pm 2$	$243 \pm 7$
07p	$38 \pm 1$	$3.092 \pm 0.001$	$101 \pm 2$	$-43 \pm 2$	$215 \pm 6$

Table 5.1: Fitting parameter for the dimuon spectra

In tab.5.1 the fitting parameters are shown. Comparing the width of the Gaussian distribution for the different datasets, the width for the datasets of 03/04, 05 and 06e are nearly the same, but the width for 07p is only the half of the others, so the resolution for the dataset of 2007 is much better.

To calculate the number of  $J/\Psi$ 's for the different datasets the normalization of the Gaussian has to be divided by the bin width. From that, together with the luminosity of the datasets, the event rate for the  $J/\Psi$  production can be calculated (tab.5.2).

dataset	$\#J/\Psi$	$L$ [ $\text{pb}^{-1}$ ]	$\frac{\#J/\Psi}{L}$ [events/ $\text{pb}^{-1}$ ]
03/04	8189	40.59	202
05	27183	135.60	200
06e	13001	54.98	236
07p	8414	43	196

Table 5.2: Event rates for the different datasets

The eventrate for 06e is higher than the others. Because of that in fig.5.7 a comparison of the muon quality for the  $J/\Psi$ -candidates of 03/04 and 06e is shown.

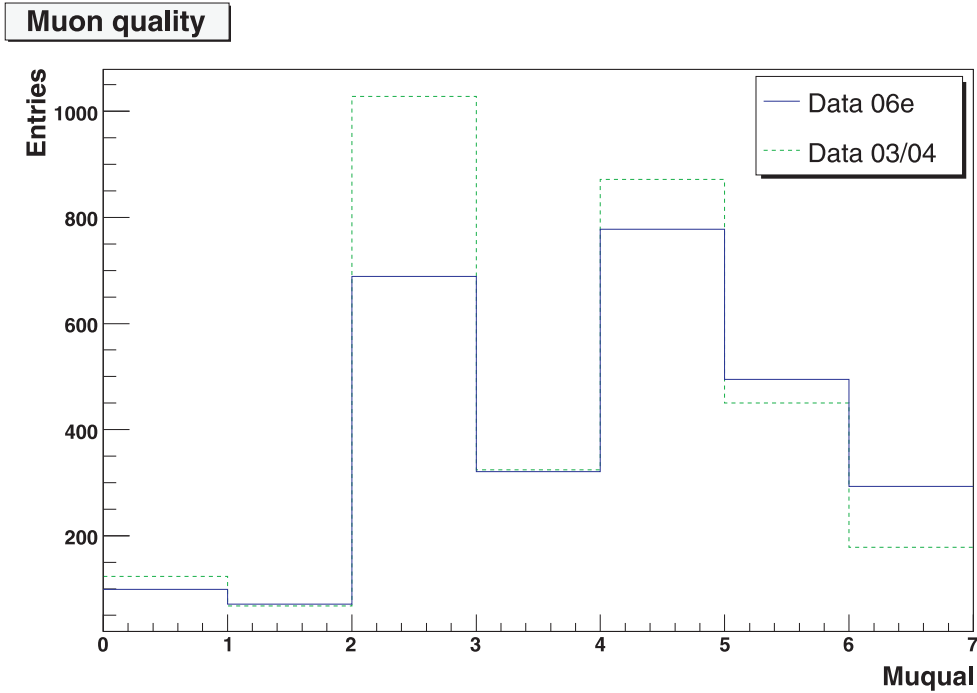


Figure 5.7: Comparison of the muon quality for 03/04 and 06e

The entries in this histograms are scaled on their luminosities to make a good comparison. For the data of 06e there were more muons with a high quality as in the data of 03/04, which is a hint that the efficiency in 06e was better than in 03/04. This might partially be due to the trigger.

## 5.4 Detector resolution

To make a statement about the detector resolution of 07 compared to 05, the  $\eta$  range for the first muon into which the  $J/\Psi$  decays was divided between  $\eta = -2$  and  $\eta = 3$  into bins of  $\Delta\eta = 0.5$ . The pseudorapidity  $\eta$  describes a spatial coordinate, which belongs to

the angle  $\theta$  between the particle and the beam axis

$$\eta = -\ln \left[ \tan \left( \frac{\theta}{2} \right) \right]. \quad (5.2)$$

The invariant mass spectra for the two muons depending on  $\eta$  for both datasets are shown in fig.A.1 and fig.A.2 with the same fits as the section before. The statistics for the range between  $2 < \eta \leq 3$  were too small, so fits weren't correct and therefore the detector resolution was only analysed for  $-2 \leq \eta \leq 2$ .

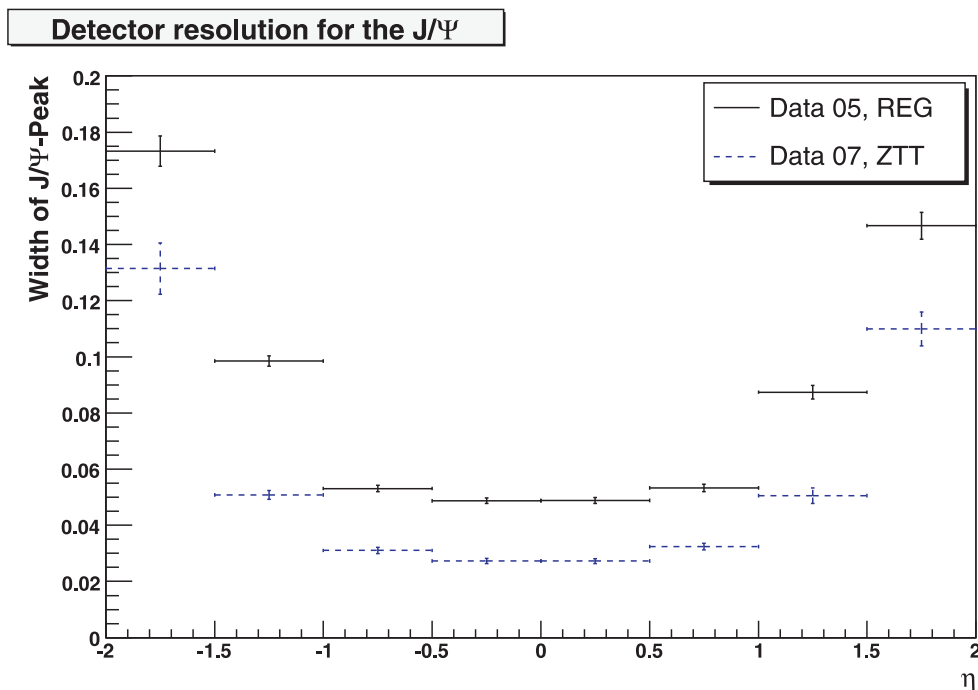


Figure 5.8: Detector resolution for the datasets of 05 and 07p

In fig.5.8 the width of the  $J/\Psi$  peak obtained from the fits is shown as a function of  $\eta$ . The resolution for 07p is better as the resolution for 05 at each point, by nearly a factor of 2. The difference in this plot between the two datasets came from the different tracking concepts, which were used here. In this case there were regular tracking for the dataset of 2005 and ZTT tracking for the dataset of 2007p, so therefore the result is that the ZTT tracking has a much better resolution.

## 5.5 Searches for $Z^0$ -candidates

### 5.5.1 $Z^0$

The  $Z^0$  has a very high mass  $m_{Z^0} = 91.1876 \pm 0.0021$  (PDG 2008), so it is not possible to find a strong  $Z^0$  signal at HERA, because of the low cross section for the  $Z^0$  production.

But with the knowledge of the mass it is possible to find some  $Z^0$  candidates and perhaps with the whole statistics some evidence for the  $Z^0$ .

At HERA the  $Z^0$  could be produced by the following four processes (fig.5.9).

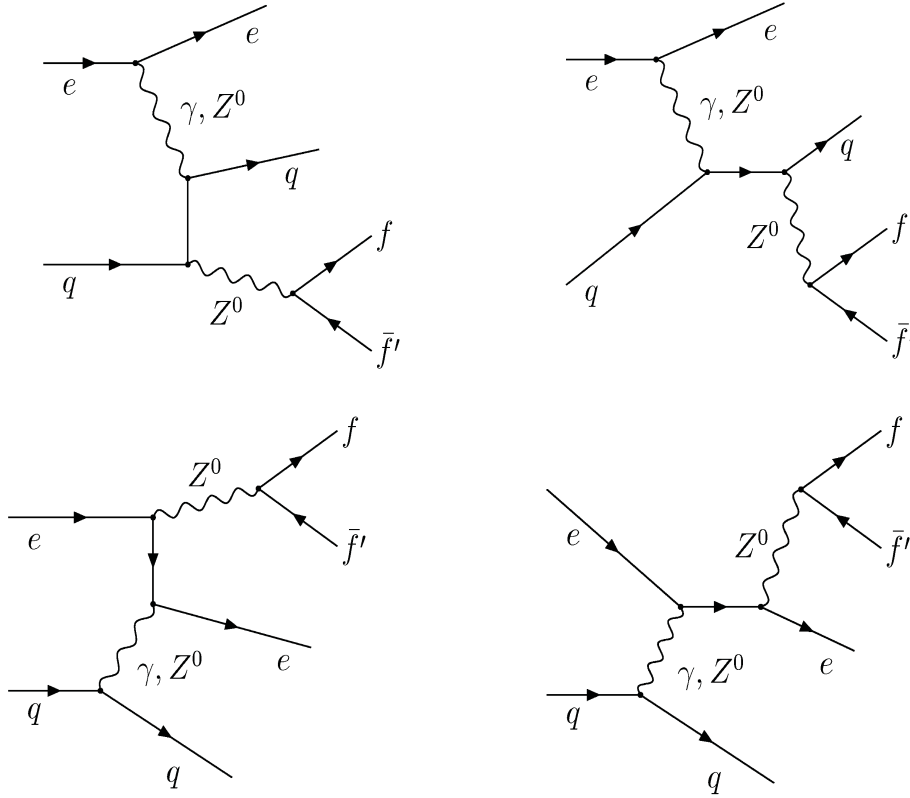


Figure 5.9: Feynmangraphs for the  $Z^0$  production at HERA [9]

For the analysis only the decay  $Z^0 \rightarrow \mu^+\mu^-$  was looked at.

### 5.5.2 Invariant mass spectrum for the two muons

dataset	run number	event number	$m_{\mu^+\mu^-}$ [GeV]
03/04	50178	70066	80.48
05	56089	83011	74.96
06e	58520	29811	80.49
06e	59588	56425	86.46
07p	61934	81637	77.31
07p	62601	163803	77.62

Table 5.3:  $Z^0$  candidates for the different datasets

In total there were 6  $Z^0$  candidates (tab.5.3) found in the different datasets between

$$70 \text{ GeV} < m_{\mu^+\mu^-} < 110 \text{ GeV} ,$$

which are shown in the event display in fig.5.10 to fig.5.15.

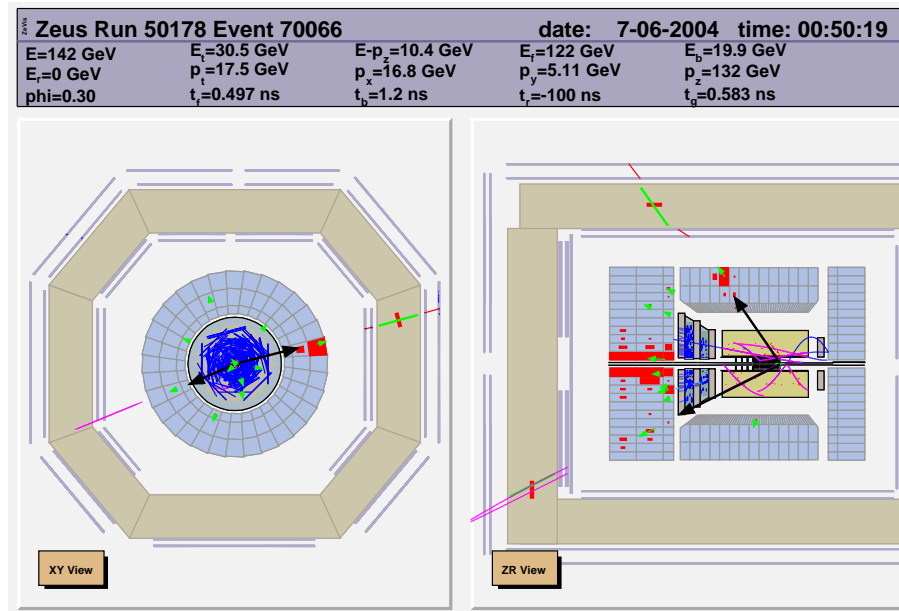


Figure 5.10:  $Z^0$  candidate for the dataset of 03/04

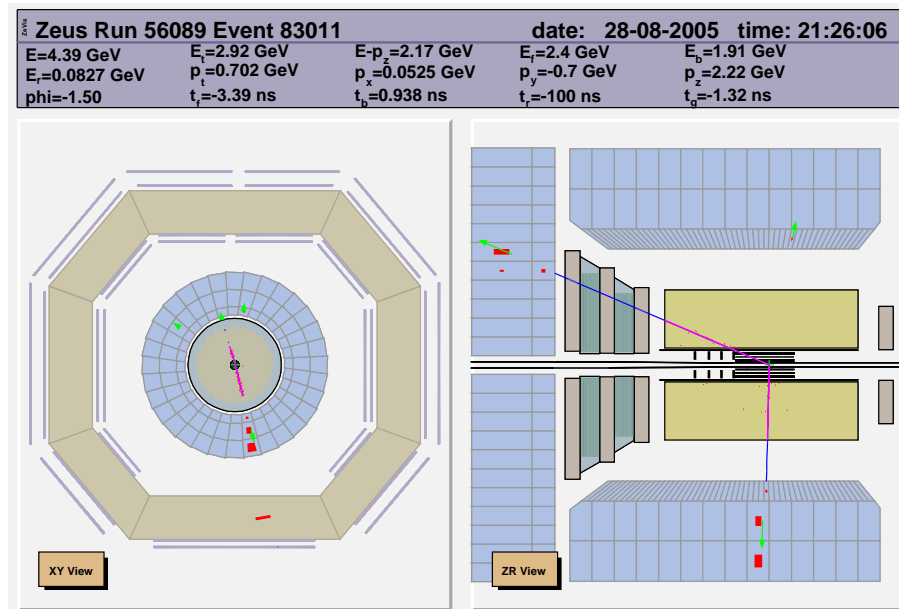


Figure 5.11:  $Z^0$  candidate for the dataset of 05

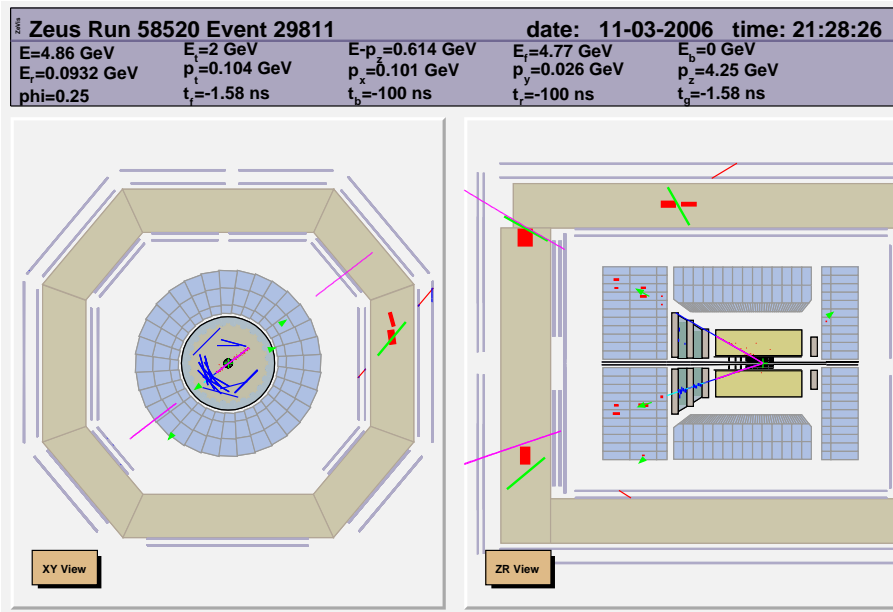


Figure 5.12:  $Z^0$  candidate for the dataset of 06e

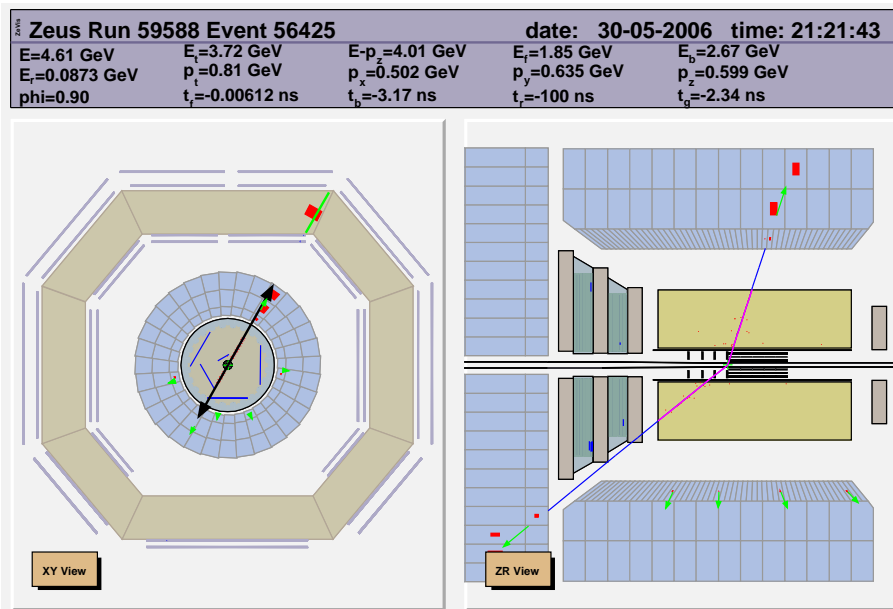
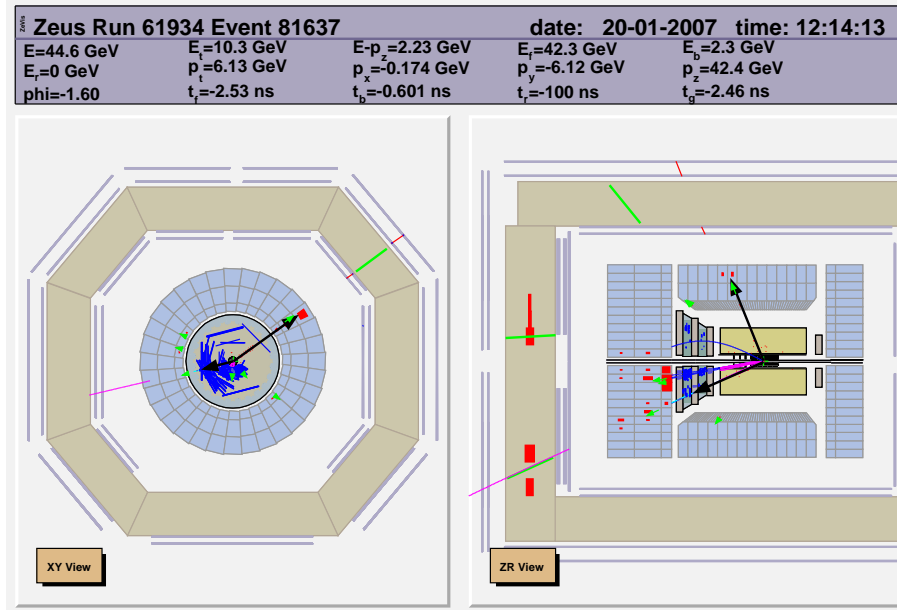
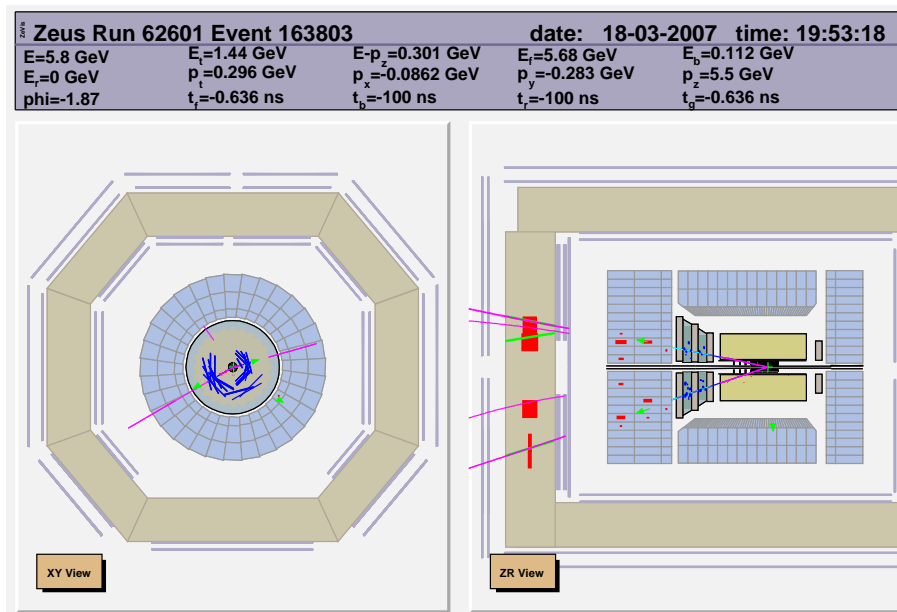


Figure 5.13:  $Z^0$  candidate for the dataset of 06e

Figure 5.14:  $Z^0$  candidate for the dataset of 07pFigure 5.15:  $Z^0$  candidate for the dataset of 07p

Additionally there were 3 other events found in this mass range, but if one looks closer to them, they don't look like a  $Z^0$  candidate.

In fig.5.16 is the invariant mass spectrum for the two muons shown, which includes all datasets to have maximal statistics.

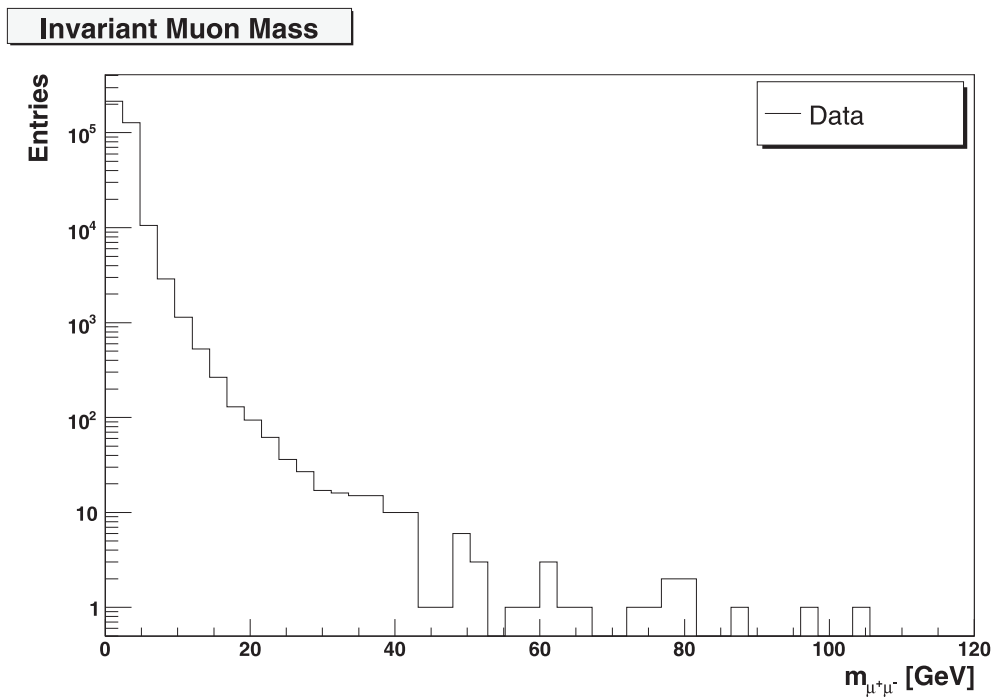


Figure 5.16: Dimuon mass spectrum for the whole HERA II data

But the statistics is still too low to say that there was evidence for the  $Z^0$ , so it is possible that some  $Z^0$ 's were produced but it can't be proven.

# 6 Tracking studies on $D^*$ <sup>1</sup>

## 6.1 $D^*$

In contrast to the production of the  $J/\Psi$ , which is a bound  $c\bar{c}$  state, mostly unbound  $c\bar{c}$  states are produced, with many possibilities of producing charm mesons, for example D-mesons, especially the  $D^{*\pm}$ . The D-mesons are very short-lived, therefore it is not possible to see them directly, the only way to evaluate them is to reconstruct them via their decay products.

The main decay channel of the  $D^{*\pm}$  is  $D^{*\pm} \rightarrow D^0\pi_s$  with a branching ratio of

$$\text{BR}(D^{*\pm} \rightarrow D^0\pi_s) = (67.7 \pm 0.5)\%.$$

The  $D^0$  has many decay channels, in this analysis there is only a look at the channel  $D^0 \rightarrow K\pi$ , which has a branching ratio of

$$\text{BR}(D^0 \rightarrow K\pi) = (3.89 \pm 0.05)\%.$$

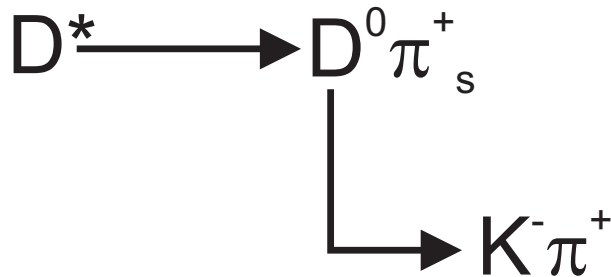


Figure 6.1: The decay channel of the  $D^*$

If both decays are combined one gets the whole decay channel of the  $D^*$  (fig.6.1) with a branching ratio of

$$\text{BR}(D^{*\pm} \rightarrow [D^0 \rightarrow K^{-/+}\pi^{+/-}]\pi^{+/-}) = (2.63 \pm 0.04)\%.$$

Therefore, for the identification of the  $D^{*\pm}$  three charged particles were required. First one identifies the  $D^0$  candidates via the calculation of the invariant mass of the  $K^{-/+}$  and  $\pi^{+/-}$  and then one calculates the invariant mass of the  $D^0$  and the  $\pi^{+/-}$ . At last, to get

---

<sup>1</sup>used literature [4] and [12]

a better resolution, one calculates the mass difference of these two invariant masses

$$\Delta M = M(K\pi\pi_s) - M(K\pi).$$

The expectation for the value is on average  $\Delta M = m_{D^*} - m_{D^0} = 0.145$  GeV (PDG). Not all particles one gets out of this reconstruction are real  $D^*$  candidates. There were also many background events which had the same final state as the the decay of the  $D^*$ . To improve the signal to background ratio there some cuts were applied.

## 6.2 The Cuts

First of all there was a pre-selection on  $M(K\pi)$  and on  $\Delta M = M(K\pi\pi_s) - M(K\pi)$  to decrease the background, because good candidates had values which were close to the values from PDG

$$M(K\pi) = (1864.84 \pm 0.18) \text{ MeV}$$

and

$$\Delta M = M(K\pi\pi_s) - M(K\pi) = (145.421 \pm 0.010) \text{ MeV}.$$

If one plots  $M(K\pi)$  as a function of  $\Delta M$  (fig.6.2) one gets a distribution, which looked like a cross and one only wants the events which were in the overlapping area of the two balks of the cross.

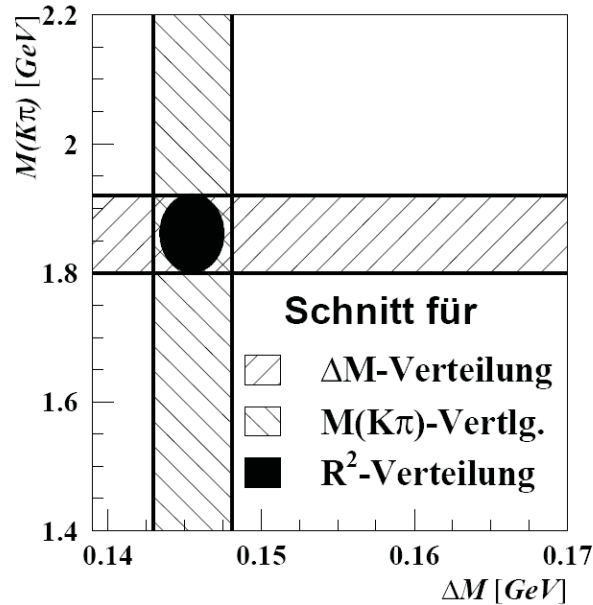


Figure 6.2:  $M(D^0)$  as a function of  $\Delta M$  [4]

Therefore, to plot  $\Delta M$ ,  $M(D^0)$  have to be between  $1.784 \text{ GeV} < M(D^0) < 1.994 \text{ GeV}$ . To reduce the background there were some additional cuts

- $|\eta(K, \pi)| < 1.7$
- $|\eta(D^*)| < 1.7$
- $|p_T(K, \pi)| > 0.4 \text{ GeV}$
- $|p_T(\pi_s)| > 0.12 \text{ GeV}$
- $p_T(D^*) > 1.5 \text{ GeV}$

### 6.3 $\Delta M$ spectrum

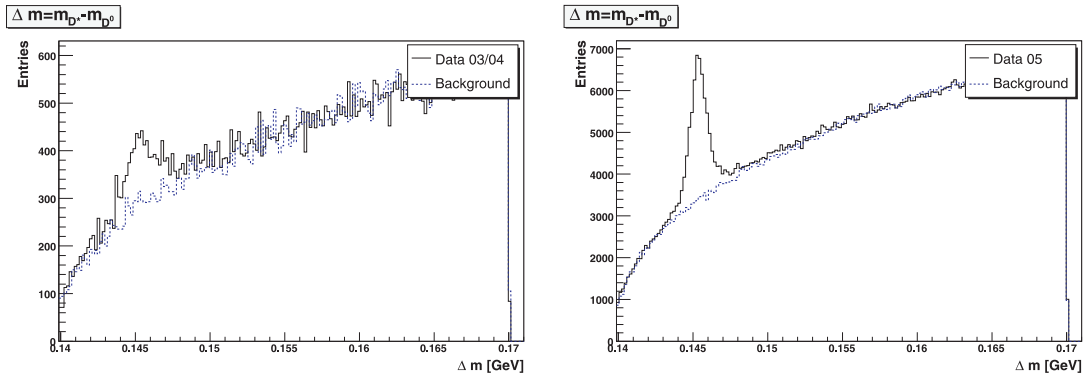


Figure 6.3:  $\Delta M$  spectrum for the dataset of a) 03/04 and b) 05

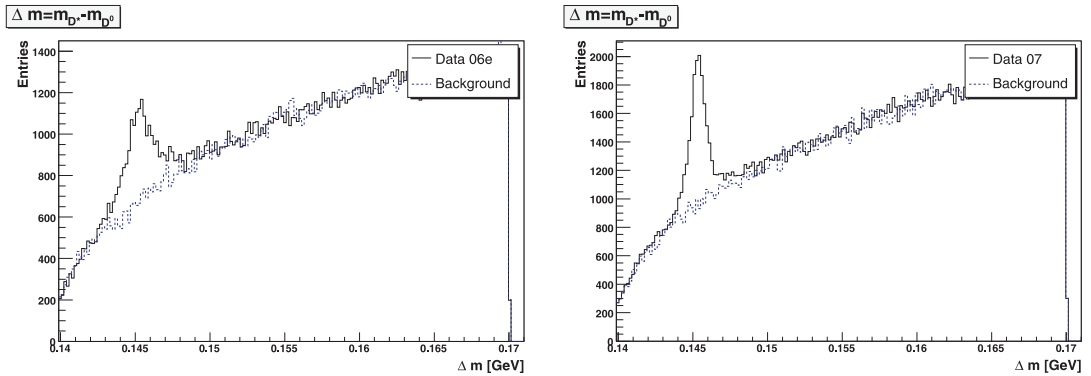


Figure 6.4:  $\Delta M$  spectrum for the dataset of a) 06e and b) 07p

In fig.6.3 to fig.6.4 the spectra for the different datasets are shown. The fact that the peaks have different heights comes from the different statistics of the datasets. In the plots also the background is shown, which can be experimentally evaluated because the distribution of wrong charged  $D^*$ -candidates (like signed pion and Kaon from the  $D^0$ ) is similar to the

real background except for a small scaling factor. Therefore, it is normalized to side bins. The number of signal events is obtained as the difference between all  $D^*$ -candidates and the number of the wrong reconstructed  $D^*$ -candidates. In tab.6.1 the scaling factor and the number of  $D^*$ 's for the different datasets are shown.

dataset	bg scaling factor	$\#D^*$
03/04	1.0097	2686
05	1.0107	32142
06e	1.0067	6856
07p	1.0072	9554

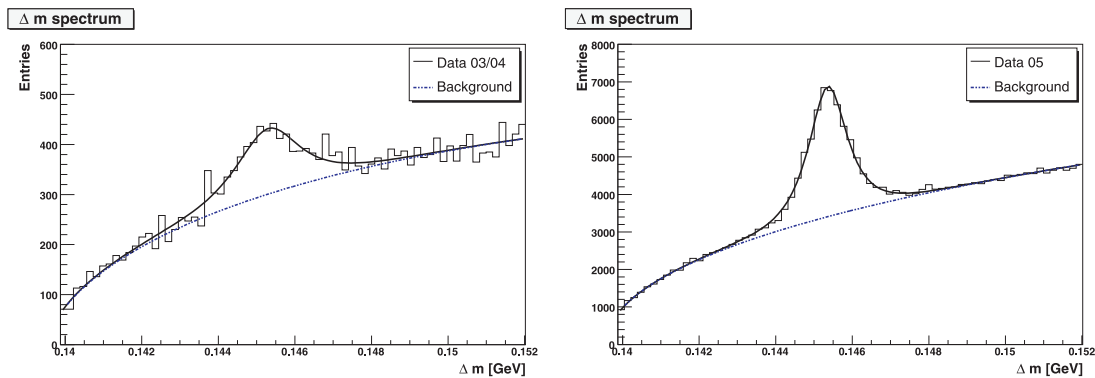
Table 6.1: Number of  $D^*$  for the different datasets

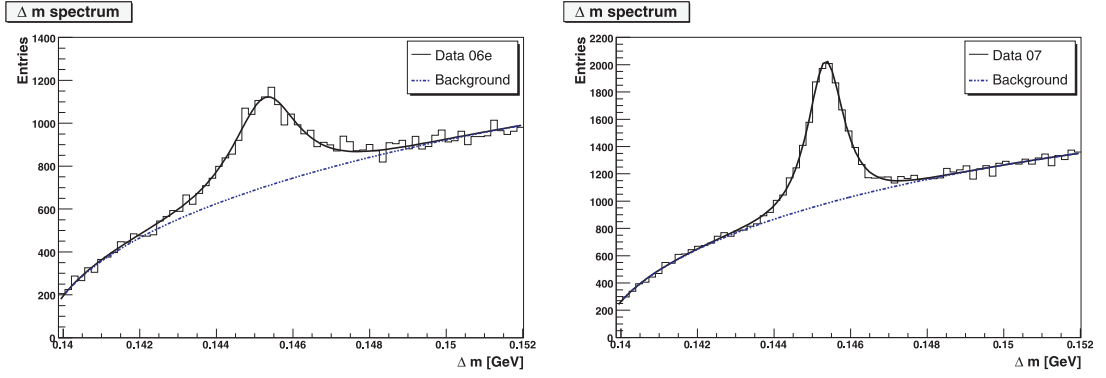
### 6.3.1 Resolution studies for the different datasets

To analyse the resolution of the different datasets, the histograms for the data fig.6.3 to fig.6.4 were fitted by the following function

$$f(x) = A \cdot (x - m_{\pi^+})^B \cdot \exp[C \cdot (x - m_{\pi^+})] + D \cdot \exp\left[-0.5 \cdot \left|\frac{x - \mu}{\sigma}\right|^{1 + \frac{1}{1 + 0.5 \cdot \left|\frac{x - \mu}{\sigma}\right|}}\right] \quad (6.1)$$

The function is composed of a so-called modified Gaussian function and a function which describes very well the distribution of the background.

Figure 6.5: Fit of the  $\Delta M$  spectrum for the dataset of a) 03/04 and b) 05

Figure 6.6: Fit of the  $\Delta M$  spectrum for the dataset of a) 06e and b) 07p

As the result of the fittings fig.6.5 and fig.6.6, tab.6.2 show the fitting parameters.

dataset	$A$	$B$	$C$	$D$	$\mu$ [MeV]	$\sigma$ [MeV]
03/04	$6715 \pm 2236$	$0.58 \pm 0.05$	$-20 \pm 11$	$131 \pm 10$	$145.30 \pm 0.10$	$0.80 \pm 0.20$
05	$44074 \pm 3420$	$0.49 \pm 0.01$	$-5 \pm 3$	$3470 \pm 46$	$145.36 \pm 0.01$	$0.48 \pm 0.01$
06e	$11015 \pm 2527$	$0.52 \pm 0.04$	$-10 \pm 8$	$417 \pm 17$	$145.28 \pm 0.04$	$0.80 \pm 0.07$
07p	$16715 \pm 2413$	$0.54 \pm 0.03$	$-13 \pm 5$	$1046 \pm 26$	$145.35 \pm 0.02$	$0.45 \pm 0.02$

Table 6.2: Fitting parameter for the  $\Delta m$  spectra

Comparing the different datasets, the width of the  $D^*$  is much smaller for 05 and 07p than for 03/04 and 06e. This also due to the difference between the types of tracking. In this case the tracking for 05 and 07p is done by ZTT and for 03/04 and 06e by REG.

## 7 Conclusion

To analyse the tracking performance for the different datasets, studies on the  $J/\Psi$  and  $D^*$  were performed. These include a closer look on the width of the mass peaks, the event rates and the detector resolution.

In summary one can say that the ZTT tracking is much better than the regular tracking and that the efficiency is also better for the last datasets. So for this analysis the reconstruction with the latest alignment is the best and there are some benchmarks for the upcoming grand reprocessing.

## 8 Acknowledgements

At first I would like to thank my supervisor Dr. Achim Geiser, who helped me very much. I would also like to thank my office colleague Danny Bot, who helped me a lot, too.

# Bibliography

- [1] [http://zms.desy.de/press/photo\\_archive/index\\_eng.html](http://zms.desy.de/press/photo_archive/index_eng.html).
- [2] <http://www-zeus.desy.de/~ibloch/ibloch.html>.
- [3] <http://www-zeus.desy.de/pictures.php3>.
- [4] Detlef Bartsch. Messung von Charm-Erzeugung in tief-inelastischer Positron-Proton-Streuung. Master's thesis, University of Bonn, 2001.
- [5] Danny Bot. Untersuchung der Nachweisbarkeit von QCD-Instantonen mit schweren Quarks in  $e^\pm p$ -Kollisionen bei HERA. Master's thesis, University of Hamburg, 2008.
- [6] Tiberiu Gabriel Grigorescu. *Measurement of Charm Production in Deep Inelastic Scattering at HERA II*. PhD thesis, University of Amsterdam, 2008.
- [7] Uwe Holm. The ZEUS Detector. Status Report, 1993.
- [8] Erik Maddox. *Study of heavy quark production at HERA using the ZEUS microvertex detector*. PhD thesis, University of Amsterdam, 2004.
- [9] Wojciech Perlanski. Analysis of dimuon events with large invariant mass in the ZEUS experiment. Heavy Flavour Meeting, August 2008.
- [10] Vincent Roberfroid. Improvement of the Kalman Filter Fit of the ZEUS experiment. ZEUS 06-10, DESY, February 2008.
- [11] Philipp Roloff. Measurement of the charm cross section using  $D^+$  and  $\Lambda_c^+$  decays in ep collisions at HERA. Master's thesis, University of Hamburg, 2007.
- [12] ZEUS Collaboration. Production of Excited Charm and Charm-Strange Mesons at HERA. ZEUS-pub-08-006, DESY, July 2008.
- [13] Jan Ziemann. Muon Efficiency Corrections in ZEUS. DESY Summerstudent Programm, 2007.

# List of Figures

2.1	The HERA-Ring [1] . . . . .	2
2.2	Feynmangraphs of the $e^\pm p$ scattering at the HERA a) neutral current b) charged current [5] . . . . .	3
2.3	The $\eta$ range of the ZEUS detector [2] . . . . .	4
2.4	Longitudinal cut through the ZEUS detector[3] . . . . .	5
2.5	Lateral cut through the ZEUS detector[3] . . . . .	5
5.1	$J/\Psi$ production and decay [13] . . . . .	9
5.2	Dimuon spectrum for the dataset of 05 . . . . .	10
5.3	Cosmic muon event . . . . .	11
5.4	The Bethe-Heitler-Process [9] . . . . .	12
5.5	Dimuon spectrum for the dataset of a) 03/04 and b) 05 . . . . .	12
5.6	Dimuon spectrum for the dataset of a) 06e and b) 07p . . . . .	13
5.7	Comparison of the muon quality for 03/04 and 06e . . . . .	14
5.8	Detector resolution for the datasets of 05 and 07p . . . . .	15
5.9	Feynmangraphs for the $Z^0$ production at HERA [9] . . . . .	16
5.10	$Z^0$ candidate for the dataset of 03/04 . . . . .	17
5.11	$Z^0$ candidate for the dataset of 05 . . . . .	17
5.12	$Z^0$ candidate for the dataset of 06e . . . . .	18
5.13	$Z^0$ candidate for the dataset of 06e . . . . .	18
5.14	$Z^0$ candidate for the dataset of 07p . . . . .	19
5.15	$Z^0$ candidate for the dataset of 07p . . . . .	19
5.16	Dimuon mass spectrum for the whole HERA II data . . . . .	20
6.1	The decay channel of the $D^*$ . . . . .	21
6.2	$M(D^0)$ as a function of $\Delta M$ [4] . . . . .	22
6.3	$\Delta M$ spectrum for the dataset of a) 03/04 and b) 05 . . . . .	23
6.4	$\Delta M$ spectrum for the dataset of a) 06e and b) 07p . . . . .	23
6.5	Fit of the $\Delta M$ spectrum for the dataset of a) 03/04 and b) 05 . . . . .	24
6.6	Fit of the $\Delta M$ spectrum for the dataset of a) 06e and b) 07p . . . . .	25
A.1	Dimuon spectra for 05 depending on $\eta$ . . . . .	32
A.2	Dimuon spectra for 07 depending on $\eta$ . . . . .	33

# List of Tables

5.1	Fitting parameter for the dimuon spectra . . . . .	13
5.2	Event rates for the different datasets . . . . .	14
5.3	$Z^0$ candidates for the different datasets . . . . .	16
6.1	Number of $D^*$ for the different datasets . . . . .	24
6.2	Fitting parameter for the $\Delta m$ spectra . . . . .	25

# Appendix A

## Measurement results

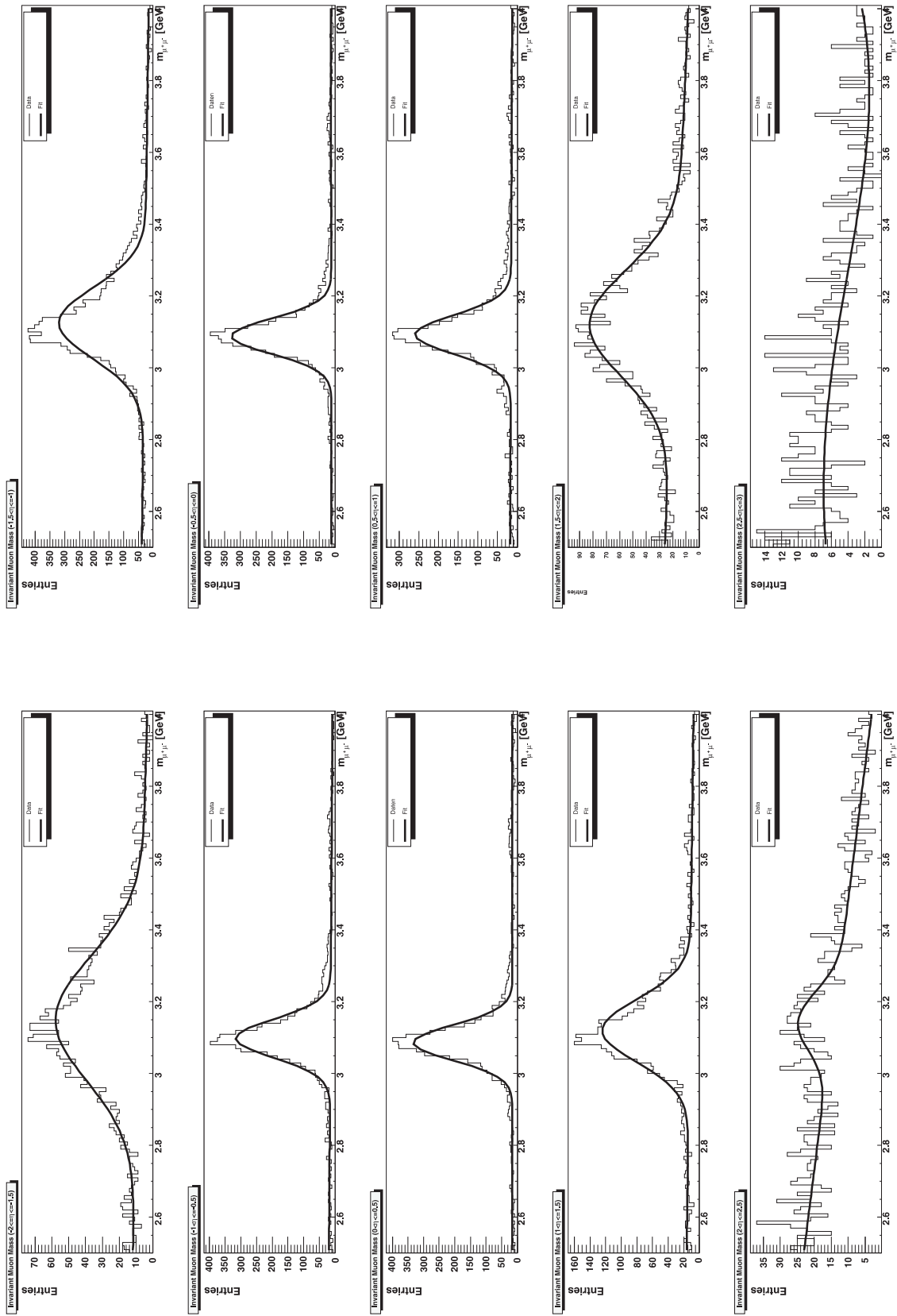


Figure A.1: Dimuon spectra for 05 depending on  $\eta$

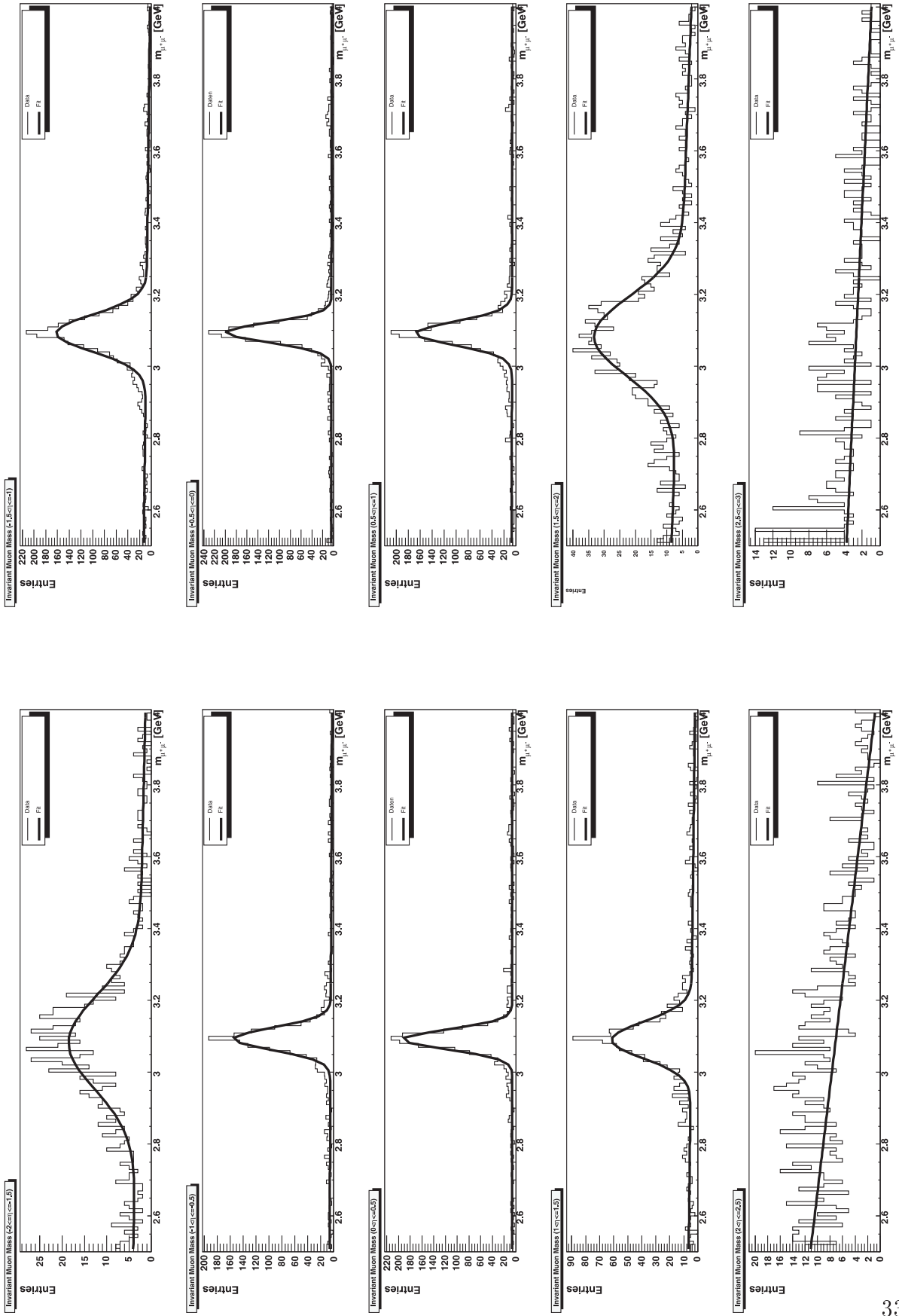


Figure A.2: Dimuon spectra for 07 depending on  $\eta$